EDGE ARTICLE

Check for updates

The oxygen-resistant [FeFe]-hydrogenase CbA5H harbors an unknown radical signal†

Melanie Heghmanns, [ID] ‡[a] Andreas Rutz, [ID] ‡[b] Yury Kutin,[a] Vera Engelbrecht,[b] Martin Winkler,[c] Thomas Happe [ID] *[b] and Müge Kasanmascheff [ID] *[a]

[FeFe]-hydrogenases catalyze the reversible conversion of molecular hydrogen into protons and electrons with remarkable efficiency. However, their industrial applications are limited by their oxygen sensitivity. Recently, it was shown that the [FeFe]-hydrogenase from *Clostridium beijerinckii* (CbA5H) is oxygen-resistant and can be reactivated after oxygen exposure. In this work, we used multifrequency continuous wave and pulsed electron paramagnetic resonance (EPR) spectroscopy to characterize the active center of CbA5H, the H-cluster. Under oxidizing conditions, the spectra were dominated by an additional and unprecedented radical species. The generation of this radical signal depends on the presence of an intact H-cluster and a complete proton transfer pathway including the bridging azadithiolate ligand. Selective ^{57}Fe enrichment combined with isotope-sensitive electron-nuclear double resonance (ENDOR) spectroscopy revealed a spin density distribution that resembles an H-cluster state. Overall, we uncovered a radical species in CbA5H that is potentially involved in the redox sensing of CbA5H.

Introduction

Molecular hydrogen is a promising alternative to fossil fuels in meeting the world's increasing energy demand.[1,2] Unlike platinum-based systems, metalloenzymes such as [FeFe]-hydrogenases use only earth-abundant metals to produce and oxidize H_2 under mild conditions and with high turnover rates (10 000 molecules per second).[3,4] The catalytic properties of these enzymes inspired the development of cheap and efficient H_2 catalysts for carbon-neutral hydrogen production.[5] Yet, their industrial application is hindered by their intrinsic O_2-sensitivity.[6,7] Despite the extensive research, engineering [FeFe]-hydrogenases with improved oxygen stability has not been entirely successful.[8]

The active site of [FeFe]-hydrogenases harbors the so-called H-cluster: a cubane [4Fe4S] cluster ([4Fe]$_H$) linked by a cysteine to a unique [2Fe2S]-subsite ([2Fe]$_H$).[3] The distal (Fe$_d$) and proximal (Fe$_p$) iron atoms of [2Fe]$_H$ are coordinated by two

CN^- and three CO ligands and are bridged by an azadithiolate (adt) ligand.[9,10] The binding of O_2 to the open coordination site at Fe$_d$ initiates a degradative process causing irreversible damage to the H-cluster.[7,11-13] Partial reduction and protonation of dioxygen, leading to H-cluster destruction, was assumed to be inherent to all [FeFe]-hydrogenases until the discovery of the hydrogenase from *Clostridium beijerinckii*, termed CbA5H (Fig. 1).[14] The H-cluster of CbA5H can reversibly switch from the oxygen-sensitive and active H$_{ox}$ state to the oxygen-stable but inactive H$_{inact}$ state.[14,15] Recently, the air-exposed crystal structure revealed that this outstanding ability is reached by the binding of a conserved cysteine residue (C367) to Fe$_d$ shielding the cofactor from O_2.[16] Structural elucidation of the H$_{inact}$ state combined with spectroscopic and electrochemical investigations[14,15] of CbA5H strongly indicate a novel oxygen resistance mechanism that does not involve direct O_2 binding to the H-cluster. Understanding the unusual oxygen resistance mechanism of CbA5H might present an important step toward facilitating the use of [FeFe]-hydrogenases as carbon-neutral energy carriers.

The work presented here expands our understanding of CbA5H and its exceptional oxygen resistance by characterizing its paramagnetic centers under oxidative and reductive conditions using isotope-sensitive electron paramagnetic resonance (EPR) spectroscopy. Along with the well-known H-cluster states in the active CbA5H, we detected an unusual radical species dominating the oxygen-treated spectra, which has not been reported in other [FeFe]-hydrogenases under similar conditions. Our investigation suggests that this radical is unique to CbA5H and potentially plays a role in the redox-sensing of the enzyme.

[a]TU Dortmund University, Department of Chemistry and Chemical Biology, Otto-Hahn-Straße 6, 44227 Dortmund, Germany. E-mail: muege.kasanmascheff@tu-dortmund.de

[b]Ruhr University Bochum, Faculty of Biology and Biotechnology, Photobiotechnology, Universitätsstr. 150, 44801 Bochum, Germany. E-mail: thomas.happe@ruhr-uni-bochum.de

[c]Technical University of Munich Campus Straubing for Biotechnology and Sustainability, Professorship for Electrobiotechnology, Uferstrasse 53, 94315 Straubing, Germany

† Electronic supplementary information (ESI) available: Material and methods, sample descriptions, experimental details and additional experimental data. See https://doi.org/10.1039/d2sc00385f
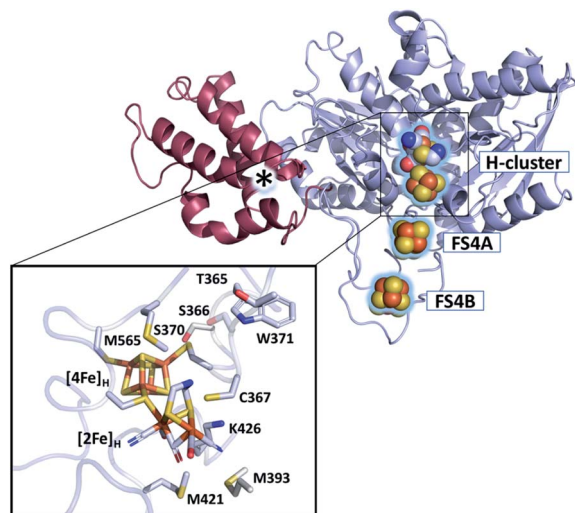
‡ Contributed equally.

Fig. 1 Structure of CbA5H (PDB ID 6TTL). X-ray structure of CbA5H displayed as a monomer with SLBB – (soluble ligand-binding beta-grasp) domain (dark-red), and H- and F-cluster containing domain (light-blue). Positions of the FeS clusters are highlighted and depicted as spheres. The asterisk indicates electron density whose nature could not be unambiguously identified yet. The lower panel shows the active site of CbA5H representing $[4Fe]_H$ and $[2Fe]_H$ embedded in the protein environment.

Results and discussion

Analysis of reduced states of apo- and holo-CbA5H

First, to investigate the paramagnetic H-cluster states, the enzyme was reduced either with H_2 or with varying concentrations of sodium dithionite (CbA5H^{NaDT}). Additionally, we performed NaDT-free control measurements (see ESI†). Analysis of the respective EPR spectra is facilitated by using elevated temperatures at which signals from fast-relaxing, accessory FeS clusters, the so-called F-clusters, are undetectable (20 K vs. 10 K spectra in Fig. 2, S1 and S2†).[17] The EPR spectrum of the active CbA5H recorded at 20 K exhibits the characteristic, well-known H-cluster states H_{ox},[18–27] H_{ox}–CO,[12,23,24,28] and H_{hyd}[29–31] (Fig. 2, S1, S2 and Tables S2 and S3†). Their presence is also confirmed via Fourier-transform infrared (FTIR) spectroscopy (Fig. S3 and ref. 15†). Interestingly, an additional signal at $g \approx 2.01$, which can be observed even up to 180 K, is also detected (Fig. S2, S4 and S5†). The origin of this unidentified species, termed R$^{•ox}$, is discussed below.

Next, to characterize the accessory FeS clusters, we employed multi-frequency EPR on the inactive apoenzyme that lacks the $[2Fe]_H$ subsite but harbors the F-clusters and $[4Fe]_H$ (apo-CbA5H) (Fig. 2, S2 and S6†). The EPR spectrum at 10 K (Fig. 2, purple trace) is dominated by a broad signal centered around $g = 1.93$. This signal is broadened beyond detection at 20 K, confirming the presence of fast-relaxing $[4Fe4S]^{1+}$ clusters (Fig. S2†).[32,33] Furthermore, its spectral features are frequency-dependent (Fig. S6†). In conjunction with the signal's significant width, the frequency dependence clearly indicates spin–spin interaction between the F-clusters.[35,36] This observation is not surprising as the clusters are adjacent (Fig. 1).[16] Spectral
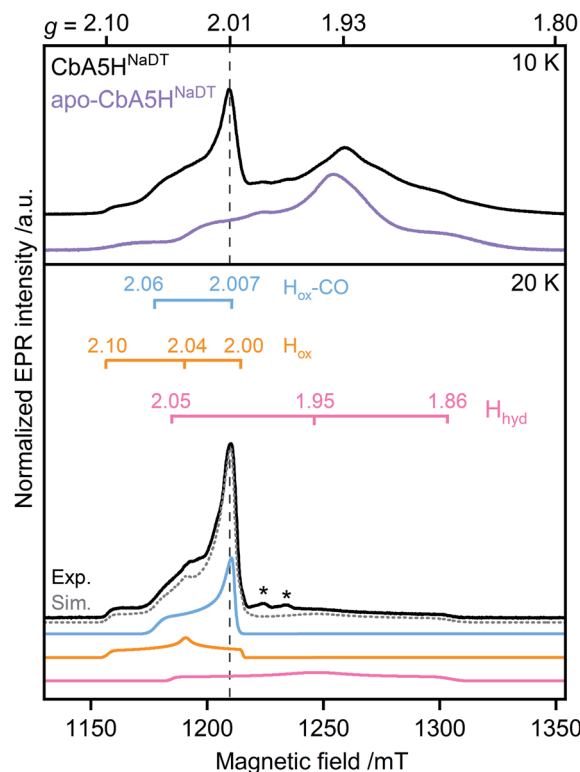

Fig. 2 Pulsed EPR spectra (34 GHz) of CbA5H (black) and apo-CbA5H (purple). The samples were reduced with 10 mM NaDT and measured at 10, and 20 K. Suppression of fast-relaxing FeS clusters at 20 K enabled the complete simulation of holo-CbA5H (dotted grey trace). H_{ox}, H_{ox}–CO, H_{hyd} and R$^{•ox}$ were included in the simulation (Fig. S1†). Details of the experiments and analysis are given in ESI.† Dashed vertical lines mark the additional signal at $g \approx 2.01$. A Mn^{2+} impurity signal is marked with asterisks.

simulation using parameters for two FeS clusters similar to those reported in the literature resulted in a good fit for the experimental apo-CbA5H^{NaDT} spectrum (Fig. S2†). Note that the R$^{•ox}$ signal found in the holoenzyme of CbA5H is absent in the apoprotein. This relates R$^{•ox}$ to the presence of an intact H-cluster.

The H_2–O_2 cycle

Unlike other [FeFe]-hydrogenases (from *Desulfovibrio desulfuricans* (*Dd*HydAB) and *Desulfovibrio vulgaris* Hildenborough), the inactive H_{inact} state of CbA5H can undergo several cycles of oxidative inactivation and reductive reactivation.[14,15] We investigated this reversible transformation by monitoring the spectral changes of the anaerobically isolated enzyme repeatedly treated with H_2 and O_2 (termed CbA5H^{H_2} and CbA5H^{O_2}, respectively) (Fig. 3 and S4†). At cryogenic temperatures, EPR spectra of CbA5H^{H_2} reveal a complex line shape (Fig. 3) arising from paramagnetic H-cluster states and F-clusters (see also Fig. 2). The overall signal intensity of CbA5H^{H_2} is reduced by approximately 40% after the first cycle (see ESI† on the H_2–O_2 cycle). This observation agrees with activity assays and FTIR
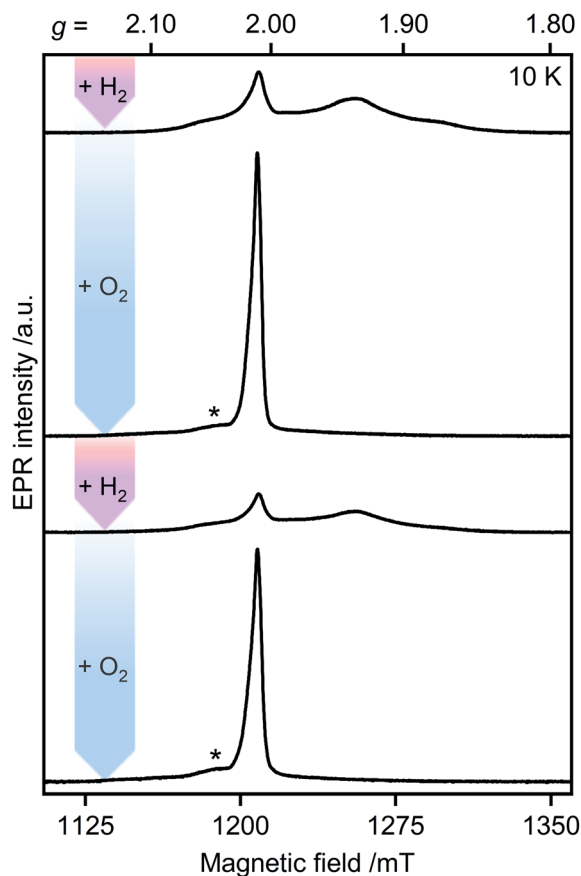
Fig. 3 Pulsed EPR spectra of CbA5H (34 GHz). As-isolated CbA5H was treated alternately with H_2 (pink arrows) and O_2 (blue arrows). Asterisks indicate residual H_{ox}–CO signals (see also ESI† on the H_2–O_2-cycle).
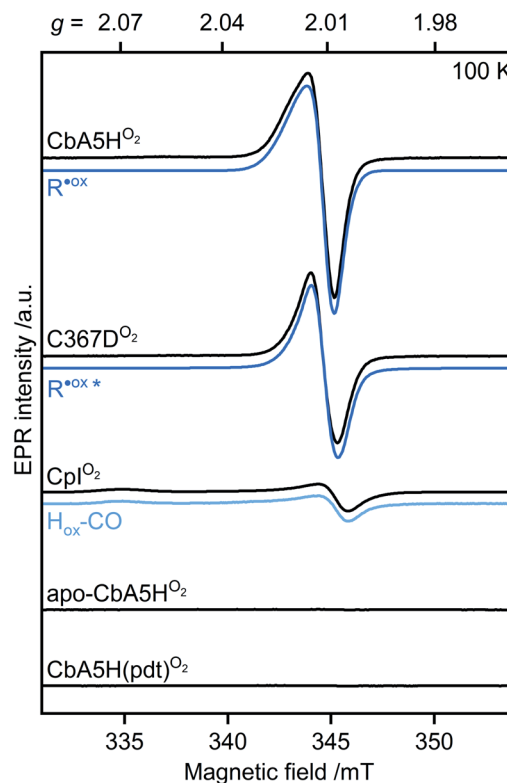

Fig. 4 Continuous-wave (cw) EPR spectra of oxygen-treated samples (9.7 GHz, $T = 100$ K). CbA5H, C367D, CpI, apo-CbA5H, and CbA5H(pdt) were treated with O_2. Blue lines represent simulations of $R^{\bullet ox}$ detected in CbA5H and variant C367D, and of H_{ox}–CO detected in CpI. The asterisk indicates a change in the $R^{\bullet ox}$ line shape for variant C367D (see Fig. S15†).

spectra (Fig. S3, S7 and ref. 15†), confirming the partial reactivation of CbA5H after O_2-treatment.

When CbA5H^{H_2} is exposed to O_2, all identified signals from the F-clusters and H-cluster disappear. This was expected as most FeS clusters are EPR-inactive in the oxidized state, and H_{inact}, the only H-cluster state present in CbA5H^{O_2} (see Fig. S3†), is suggested to be EPR-silent.[15] The EPR spectra of CbA5H^{O_2} (Fig. 3), however, are dominated by the nearly isotropic signal at $g = 2.01$ (Fig. 4). Its EPR signature is distinct from typical signals of H_{ox}–CO and degraded FeS clusters (Fig. S4 and S7†). Its three principal g-values were determined as $g = 2.019, 2.010, 2.006$ via a global fit at the X- and Q-band frequencies (see Table S2† for details). Surprisingly, its intensity decreases only by 5–13% after two H_2–O_2 cycles and cryo-annealing, while the amount of active protein drops significantly (ESI on the H_2–O_2 cycle, Fig. 3 and S4–S7†). Even though $R^{\bullet ox}$ is present in CbA5H^{H_2}, its EPR-intensity is considerably higher in the oxidized enzyme (Fig. 3 and S4†). The high stability of $R^{\bullet ox}$ contradicts the observed degradation of H_{inact} during the cycle, as shown via FTIR (Fig. S3†), indicating that the H_{inact} state itself is not the source of $R^{\bullet ox}$. Moreover, the generation of $R^{\bullet ox}$ by treatment with the mild oxidant hexamine ruthenium(III) chloride (HAR) showed that O_2 is not the only catalyst triggering its formation (Fig. S9†). Similar results were reported for the generation of H_{inact},[15] emphasizing the

connection between H_{inact} formation and the $R^{\bullet ox}$ signal. This is reminiscent of the EPR signals observed for the proximal [4Fe3S] cluster of O_2-tolerant [NiFe]-hydrogenases under oxidative conditions, even in the absence of O_2,[37] which turn out to be a strong indicator for the underlying O_2 tolerance mechanism. These intriguing properties of the $R^{\bullet ox}$ species prompted us to investigate its identity further.

Investigation of $R^{\bullet ox}$ formation under various conditions

First, we analyzed the EPR spectra of O_2-exposed CbA5H compared to CpI (Fig. 4 and S10†). CpI, a 'standard' [FeFe]-hydrogenase, was purified and oxidized using the same procedure for CbA5H. In agreement with reported CpI data,[34] $R^{\bullet ox}$ was not detected in EPR spectra of CpI^{O_2}, demonstrating that the signal is unique to CbA5H. These data also exclude the possibility of $R^{\bullet ox}$ being an artifact related to the protein preparation procedures or a radical species generated due to external factors such as the buffers used. This conclusion is further supported by (i) the almost identical EPR signature of $R^{\bullet ox}$ in aerobically and anaerobically isolated CbA5H (Fig. S11†) and (ii) the absence of the $R^{\bullet ox}$ signal in EPR spectra of apo-CbA5H (reduced or oxidized). The only signal detected in the oxidized apoenzyme originates from a $[3Fe4S]^+$ cluster in substoichiometric amounts, possibly from mild oxidative damage to the FeS clusters (Fig. S6, S8 and S12†).

We, therefore, explored whether an active enzyme is necessary to generate $R^{\cdot ox}$. Apo-CbA5H was matured with a chemically altered cofactor ($[Fe_2(pdt)(CO_4)(CN_2)]^{2-}$, CbA5H(pdt)) yielding a catalytically inactive enzyme due to the non-protonatable bridgehead.[35] This artificial ligand does not interfere with the native structure of the hydrogenases but disrupts the proton-transfer pathway to and from Fe_d.[36,38,39] The complex EPR spectrum of H_2-reduced CbA5H(pdt) (Fig. S13†) resembles the corresponding spectrum reported for CpI(pdt).[17] The spectrum of O_2-treated CbA5H(pdt) shows sub-stoichiometric amounts of a $[3Fe4S]^+$ cluster (Fig. S13†), similar to the one detected in apo-CbA5H^{O_2}. Strikingly, none of the EPR spectra recorded for CbA5H(pdt) exhibit the $R^{\cdot ox}$ signal (Fig. 4 and S13†), although the formation of the H_{inact} state in CbA5H(pdt) was verified by FTIR measurements (Fig. S14†). This again excludes H_{inact} as the source of $R^{\cdot ox}$.

To this point, our results on EPR characteristics (g-values and temperature-dependency) of $R^{\cdot ox}$ hint at a protein-based radical species whose generation is dependent on the presence of an active H-cluster and the native adt ligand, ensuring an intact proton transfer pathway. The cysteine residue C367 is one of the closest amino acids to the H-cluster and is involved in the H_{inact} formation.[16] Therefore, we investigated whether the oxidation of C367 results in the $R^{\cdot ox}$ signal.

We recorded EPR spectra of the O_2-treated CbA5H in which C367 is replaced with aspartate (C367D) (Fig. 4 and S15†). This variant prevented the formation of the H_{inact} state while retaining 20% of the H_2-production activity compared to the wild-type enzyme.[16] Temperature-dependent spectra exhibit the $R^{\cdot ox}$ signal but with a narrower line shape and decreased intensity. Although these results exclude C367 as the source of $R^{\cdot ox}$, they show that the identity of residue 367 affects its electronic structure.

Furthermore, the characteristics of our EPR and UV-vis data conflict with those of typical (i) amino acid radicals, (ii) sulfur-based radicals, (iii) peroxyl radicals, and (iv) semiquinone radicals (Fig. S16 and ESI Discussion† on the identity of $R^{\cdot ox}$). Yet, an unusual organic radical near, on, or bound to the H-cluster with anomalous spectroscopic properties, as observed with the tryptophane cation radical found in cytochrome c peroxidase[40,41] cannot be ruled out. Candidates that might be considered are residues M393, S370 or M565, M421, and W371 (Fig. 1), of which the last three represent highly conserved positions among other [FeFe]-hydrogenases.

^{57}Fe-labeling and isotope-sensitive studies of $R^{\cdot ox}$

EPR studies combined with ^{57}Fe labeling provided invaluable information on iron-containing metalloproteins, including elucidation of the electronic structure of H-cluster states from different organisms.[9,27,42,43] The presence of a ^{57}Fe nucleus with a nuclear spin $I = \frac{1}{2}$ results in EPR line broadening due to hyperfine interaction (hfi). To investigate whether $R^{\cdot ox}$ is associated with the H-cluster, we selectively labeled the apoprotein ([4Fe]$_H$ and F-clusters) with ^{57}Fe and subsequently matured it with ^{56}Fe–[2Fe]$_H$. The g-value of $R^{\cdot ox}$ did not change upon labeling. However, ^{57}Fe enrichment resulted in EPR line
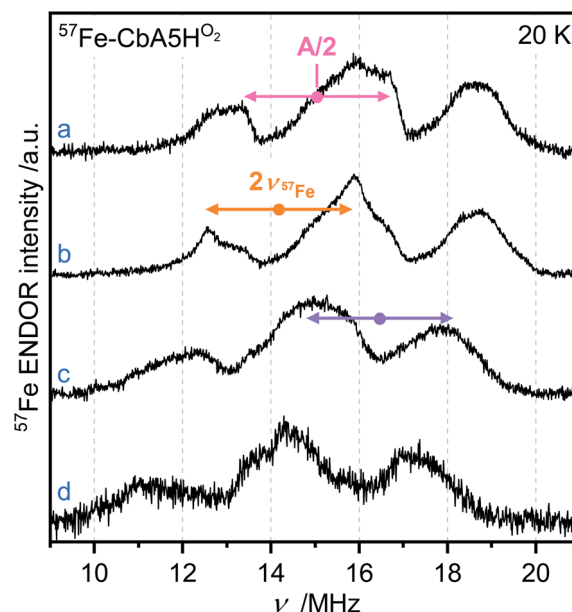

Fig. 5 Orientation-selective Davies ENDOR spectra of ^{57}Fe-labeled CbA5H^{O_2} recorded at 20 K, Q-band and (a) $g = 2.008$ (b) $g = 2.012$ (c) $g = 2.018$ (d) $g = 2.022$. At least three different ^{57}Fe hyperfine couplings are observable, centered at $A/2$ (dots), and split by twice the Larmor frequency (arrows). All experimental details are given in ESI.†

broadening of the $R^{\cdot ox}$ spectra due to strong hfis between ^{57}Fe nuclei and $R^{\cdot ox}$ (Fig. S17†).

Next, we recorded orientation-selective ^{57}Fe electron-nuclear double resonance (ENDOR) spectra of $R^{\cdot ox}$ (Fig. 5). The ENDOR line shape shows three broad features symmetrically centered around $|A|/2$ (A is the hyperfine coupling constant) and split by twice the Larmor frequency $\nu_{57_{Fe}}$ due to strong hfis with several ^{57}Fe nuclei. At least three ^{57}Fe nuclei needed to be introduced to simulate the experimental ENDOR line shape (Fig. S18†). At this point, however, a complete and unique analysis of the orientation-selective ^{57}Fe ENDOR pattern is not possible, as only a few features of the overlapping signals are resolved at Q-band. Nonetheless, the hf couplings of all observed ^{57}Fe nuclei are in the range of 25–35 MHz, very similar to those observed for the [4Fe]$_H$ subcluster in the H_{ox}–CO state from other hydrogenases.[9,43] These data suggest that $R^{\cdot ox}$ is either a unique H-cluster state or located close to the intact H-cluster and thus coupled to [4Fe]$_H$. Note that the F-clusters in their native conformation can be excluded as the source of observed hfis because (i) $R^{\cdot ox}$ is not generated in the absence of an intact H-cluster, i.e., in apo-CbA5H, (ii) slow relaxation behavior of $R^{\cdot ox}$ is inconsistent with a typical [4Fe4S]$^{1+}$ cluster, (iii) substituting the C367 residue residing close to [2Fe]$_H$ perturbs the EPR line shape of $R^{\cdot ox}$, and (iv) the isotropic hfis determined for $R^{\cdot ox}$ are significantly different from the ones observed for the standard [4Fe4S]$^{1+}$ clusters displaying $|A_{iso}|$ of around 15 MHz for their ferrous Fe^{2+}–Fe^{2+} pair.[44]

Next, we performed orientation-selective proton (^{1}H) ENDOR experiments on $R^{\cdot ox}$ (Fig. S19†). The spectra revealed overlapping signals due to contributions from several protons having hfis not larger than 9 MHz. As our ^{57}Fe EPR data showed

effective spin density on the H-cluster, we compared ^{1}H ENDOR spectra of R$^{•ox}$ with those of H$_{ox}$, H$_{ox}$–CO, and H$_{hyd}$ from different [FeFe]-hydrogenases.[45–47] As with the ^{57}Fe data, the strength of the hfis and the spectral shape of R$^{•ox}$ ^{1}H ENDOR resemble those detected with H$_{ox}$–CO assigned to β-protons of the cysteine ligands of [4Fe]$_H$.[45–47]

To demonstrate that the detected ^{57}Fe and ^{1}H hfis do not arise from the underlying H$_{ox}$–CO species, we recorded FTIR spectra for oxygen-treated ^{57}Fe–CbA5H (Fig. S3†) and ^{1}H ENDOR spectra with CbA5H^{air} whose EPR spectrum is composed of R$^{•ox}$ and H$_{ox}$–CO (Fig. S19†). The absence of an H$_{ox}$–CO FTIR signature in ^{57}Fe–CbA5H^{O_2} and the presence of additional features in ^{1}H ENDOR spectra of CbA5H^{air} showed that the observed hfis belong to R$^{•ox}$. The similarities detected in hfis strongly imply a similar spin density distribution for R$^{•ox}$ and H$_{ox}$–CO, which features a paramagnetic [2Fe]$_H$ ($S = 1/2$) exchange coupled to the diamagnetic [4Fe]$_H{}^{2+}$.

Interestingly, the F-cluster-truncated form of the [FeFe]-hydrogenase from *Megasphaera elsdenii*, harboring the H-cluster, displayed an EPR signal similar to R$^{•ox}$ upon CO-treatment.[6] This signal was attributed to the H$_{ox}$–CO state. However, the EPR signature differs substantially from the H$_{ox}$–CO state observed for the as-isolated enzyme and other known [FeFe]-hydrogenases. As the FTIR spectrum of this redox state was similar to those of other hydrogenases, the unusual change in the EPR spectrum could not be explained. Here, we can exclude the well-known H$_{ox}$–CO state as the origin of the R$^{•ox}$ signal because we can distinguish the features of H$_{ox}$–CO and R$^{•ox}$ in our temperature-dependent EPR and ENDOR data (Fig. S8 and S19†).

Lastly, we investigated the presence of exchangeable protons by recording ^{1}H ENDOR spectra of R$^{•ox}$ in the D$_2$O buffer. Indeed, we detected differences in the proton ENDOR spectra of R$^{•ox}$ in H$_2$O or D$_2$O buffers. In addition, the ^{2}H Mims ENDOR spectrum revealed at least two proton hfis arising from the exchangeable protons (see Fig. S19–S20†). These associate R$^{•ox}$ with coordinating water or solvent-derived protonated species, *e.g.*, an amino acid residue with an exchangeable proton. One might hypothesize that the flexible loop around the H-cluster of CbA5H facilitates the movement of conserved water/s that is part of the proton-transfer pathway (see Fig. S6 in ref. 16†).

Overall, our EPR and ENDOR data show a spin density distribution at the H-cluster similar to the H$_{ox}$–CO state and exclude C367 and H$_{inact}$ as the source of R$^{•ox}$. Therefore, it would be intriguing to interpret R$^{•ox}$ as an H-cluster state distinct from H$_{ox}$, H$_{ox}$–CO, H$_{inact}$, and H$_{hyd}$. However, the absence of the corresponding FTIR data that could be associated with R$^{•ox}$ prevents an unambiguous assignment at this moment.

Conclusions

In this study, we provided direct spectroscopic evidence for the presence of an unprecedented radical species in CbA5H, named R$^{•ox}$. We showed that the formation of R$^{•ox}$ under oxidizing conditions is dependent on the presence of an active H-cluster harboring the native adt ligand that ensures an intact proton transfer pathway. While advanced spectroscopic and biochemical studies are underway aiming to reveal the identity of R$^{•ox}$, the combined results of our temperature-dependent and isotope-sensitive spectroscopic investigations already narrow down its location within the protein to either the H-cluster or its immediate vicinity. In line with the early onset of anaerobic oxidative inactivation and the formation of H$_{inact}$, the R$^{•ox}$ signal appears either in the presence of O$_2$ or upon applying oxidative conditions in the absence of it. Similar to the intact proton transfer pathway to Fed, R$^{•ox}$ formation seems to be part of the redox sensing process that determines the reversible formation of H$_{inact}$ in CbA5H.

Data availability

All experimental data associated with the paper can be found in the article or in the ESI.†

Author contributions

MH (first shared author): data curation, formal analysis, investigation, writing – original draft. AR (first shared author): data curation, formal analysis, investigation. YK: supervision, data curation, validation, writing – review & editing. VE: writing – review & editing. MW: conceptualization, writing – review & editing. TH (corresponding author): supervision, validation, resources, funding acquisition, conceptualization, writing – review & editing. MK (corresponding author): methodology, validation, supervision, resources, funding acquisition, conceptualization, writing – original draft, review & editing.

Conflicts of interest

There are no conflicts to declare.

Acknowledgements

References

1 J. Tollefson, *Nature*, 2010, **464**, 1262–1264.
2 M. K. Singla, P. Nijhawan and A. S. Oberoi, *Environ. Sci. Pollut. Res.*, 2021, **28**, 15607–15626.
3 W. Lubitz, H. Ogata, O. Rüdiger and E. Reijerse, *Chem. Rev.*, 2014, **114**, 4081–4148.
4 B. R. Glick, W. G. Martin and S. M. Martin, *Can. J. Microbiol.*, 1980, **26**, 1214–1223.

5 S. Gao, W. Fan, Y. Liu, D. Jiang and Q. Duan, *Int. J. Hydrogen Energy*, 2020, **45**, 4305–4327.

6 G. Caserta, C. Papini, A. Adamska-Venkatesh, L. Pecqueur, C. Sommer, E. Reijerse, W. Lubitz, C. Gauquelin, I. Meynial-Salles, D. Pramanik, V. Artero, M. Atta, M. del Barrio, B. Faivre, V. Fourmond, C. Léger and M. Fontecave, *J. Am. Chem. Soc.*, 2018, **140**, 5516–5526.

7 J. Esselborn, L. Kertess, U. P. Apfel, E. Hofmann and T. Happe, *J. Am. Chem. Soc.*, 2019, **141**, 17721–17728.

8 A. Dubini and D. Gonzalez-Ballester, in *Algae Biotechnology*, 2016, pp. 165–193.

9 A. Silakov, E. J. Reijerse, S. P. J. Albracht, E. C. Hatchikian and W. Lubitz, *J. Am. Chem. Soc.*, 2007, **129**, 11447–11458.

10 Z.-P. P. Liu and P. Hu, *J. Am. Chem. Soc.*, 2002, **124**, 5175–5182.

11 A. Kubas, C. Orain, D. De Sancho, L. Saujet, M. Sensi, C. Gauquelin, I. Meynial-Salles, P. Soucaille, H. Bottin, C. Baffert, V. Fourmond, R. B. Best, J. Blumberger and C. Léger, *Nat. Chem.*, 2017, **9**, 88–95.

12 K. D. Swanson, M. W. Ratzloff, D. W. Mulder, J. H. Artz, S. Ghose, A. Hoffman, S. White, O. A. Zadvornyy, J. B. Broderick, B. Bothner, P. W. King and J. W. Peters, *J. Am. Chem. Soc.*, 2015, **137**, 1809–1816.

13 S. Mebs, R. Kositzki, J. Duan, L. Kertess, M. Senger, F. Wittkamp, U. P. Apfel, T. Happe, S. T. Stripp, M. Winkler and M. Haumann, *Biochim. Biophys. Acta, Bioenerg.*, 2018, **1859**, 28–41.

14 S. Morra, M. Arizzi, F. Valetti and G. Gilardi, *Biochemistry*, 2016, **55**, 5897–5900.

15 P. S. Corrigan, J. L. Tirsch and A. Silakov, *J. Am. Chem. Soc.*, 2020, **142**, 12409–12419.

16 M. Winkler, J. Duan, A. Rutz, C. Felbek, L. Scholtysek, O. Lampret, J. Jaenecke, U.-P. Apfel, G. Gilardi, F. Valetti, V. Fourmond, E. Hofmann, C. Léger and T. Happe, *Nat. Commun.*, 2021, **12**, 756.

17 J. H. Artz, D. W. Mulder, M. W. Ratzloff, C. E. Lubner, O. A. Zadvornyy, A. X. Levan, S. G. Williams, M. W. W. Adams, A. K. Jones, P. W. King and J. W. Peters, *J. Am. Chem. Soc.*, 2017, **139**, 9544–9550.

18 H. J. Grande, W. R. Dunham, B. Averill, C. van Dijk and R. H. Sands, *Eur. J. Biochem.*, 1983, **136**, 201–207.

19 W. R. Hagen, A. van Berkel-Arts, K. M. Krüse-Wolters, W. R. Dunham and C. Veeger, *FEBS Lett.*, 1986, **201**, 158–162.

20 M. W. Adams, *J. Biol. Chem.*, 1987, **262**, 15054–15061.

21 A. J. Pierik, W. R. Hagen, J. S. Redeker, R. B. G. Wolbert, M. Boersma, M. F. J. M. Verhagen and H. J. Grande, *Eur. J. Biochem.*, 1992, **209**, 63–72.

22 B. Bennett, B. J. Lemon and J. W. Peters, *Biochemistry*, 2000, **39**, 7455–7460.

23 S. P. J. Albracht, W. Roseboom and E. C. Hatchikian, *J. Biol. Inorg Chem.*, 2006, **11**, 88–101.

24 C. Kamp, A. Silakov, M. Winkler, E. J. Reijerse, W. Lubitz and T. Happe, *Biochim. Biophys. Acta, Bioenerg.*, 2008, **1777**, 410–416.

25 A. Adamska, A. Silakov, C. Lambertz, O. Rüdiger, T. Happe, E. Reijerse and W. Lubitz, *Angew. Chem., Int. Ed.*, 2012, **51**, 11458–11462.

26 G. Caserta, L. Pecqueur, A. Adamska-Venkatesh, C. Papini, S. Roy, V. Artero, M. Atta, E. Reijerse, W. Lubitz and M. Fontecave, *Nat. Chem. Biol.*, 2017, **13**, 779–784.

27 G. Rao and R. D. Britt, *Inorg. Chem.*, 2018, **57**, 10935–10944.

28 W. Roseboom, A. L. De Lacey, V. M. Fernandez, E. C. Hatchikian and S. P. J. Albracht, *J. Biol. Inorg Chem.*, 2006, **11**, 102–118.

29 D. W. Mulder, M. W. Ratzloff, M. Bruschi, C. Greco, E. Koonce, J. W. Peters and P. W. King, *J. Am. Chem. Soc.*, 2014, **136**, 15394–15402.

30 D. W. Mulder, Y. Guo, M. W. Ratzloff and P. W. King, *J. Am. Chem. Soc.*, 2017, **139**, 83–86.

31 M. Winkler, M. Senger, J. Duan, J. Esselborn, F. Wittkamp, E. Hofmann, U. P. Apfel, S. T. Stripp and T. Happe, *Nat. Commun.*, 2017, **8**(16115).

32 R. Cammack, *Adv. Inorg. Chem.*, 1992, **38**, 281–322.

33 H. Rupp, K. K. Rao, D. O. Hall and R. Cammack, *Nat. Commun.*, 1978, **537**, 255–269.

34 M. W. W. Adams, *Biochim. Biophys. Acta, Bioenerg.*, 1990, **1020**, 115–145.

35 G. Berggren, A. Adamska, C. Lambertz, T. R. Simmons, J. Esselborn, M. Atta, S. Gambarelli, J. M. Mouesca, E. Reijerse, W. Lubitz, T. Happe, V. Artero and M. Fontecave, *Nature*, 2013, **499**, 66–69.

36 M. M. Roessler, R. M. Evans, R. A. Davies, J. Harmer and F. A. Armstrong, *J. Am. Chem. Soc.*, 2012, **134**, 15581–15594.

37 J. Esselborn, C. Lambertz, A. Adamska-Venkatesh, T. Simmons, G. Berggren, J. Noth, J. Siebel, A. Hemschemeier, V. Artero, E. Reijerse, M. Fontecave, W. Lubitz and T. Happe, *Nat. Chem. Biol.*, 2013, **9**, 607–609.

38 W. Lubitz, E. Reijerse and M. van Gastel, *Chem. Rev.*, 2007, **107**, 4331–4365.

39 J. Esselborn, N. Muraki, K. Klein, V. Engelbrecht, N. Metzler-Nolte, U. P. Apfel, E. Hofmann, G. Kurisu and T. Happe, *Chem. Sci.*, 2016, **7**, 959–968.

40 M. Sivaraja, D. B. Goodin, M. Smith and B. M. Hoffman, *Science*, 1989, **245**, 738–740.

41 A. L. P. Houseman, P. E. Doan, D. B. Goodin and B. M. Hoffman, *Biochemistry*, 1993, **32**, 4430–4443.

42 C. V. Popescu and E. Münck, *J. Am. Chem. Soc.*, 1999, **121**, 7877–7884.

43 R. Gilbert-Wilson, J. F. Siebel, A. Adamska-Venkatesh, C. C. Pham, E. Reijerse, H. Wang, S. P. Cramer, W. Lubitz and T. B. Rauchfuss, *J. Am. Chem. Soc.*, 2015, **137**, 8998–9005.

44 J. M. Mouesca, L. Noodleman, D. A. Case and B. Lamotte, *Inorg. Chem.*, 1995, **34**, 4347–4359.

45 J. Telser, M. J. Benecky, M. W. Adams, L. E. Mortenson and B. M. Hoffman, *J. Biol. Chem.*, 1987, **262**, 6589–6594.

46 A. Silakov, E. J. Reijerse and W. Lubitz, *Eur. J. Inorg. Chem.*, 2011, 1056–1066.

47 A. Adamska-Venkatesh, T. R. Simmons, J. F. Siebel, V. Artero, M. Fontecave, E. Reijerse and W. Lubitz, *Phys. Chem. Chem. Phys.*, 2015, **17**, 5421–5430.